Journal of Materials Chemistry C

A Portable Fiber Optic Sensor for the Luminescent Sensing of Cobalt Ions Using Carbon Dots

Journal:	*Journal of Materials Chemistry C*
Manuscript ID	TC-ART-06-2022-002560.R1
Article Type:	Paper
Date Submitted by the Author:	10-Oct-2022
Complete List of Authors:	Crawford, Scott; National Energy Technology Laboratory, Functional Materials Kim, Ki-Joong; National Energy Technology Laboratory, ; AECOM, Baltrus, John; National Energy Technology Laboratory,

ARTICLE

A Portable Fiber Optic Sensor for the Luminescent Sensing of Cobalt Ions Using Carbon Dots

Received 00th January 20xx,
Accepted 00th January 20xx

DOI: 10.1039/x0xx00000x

Scott E. Crawford,*[a,b] Ki-Joong Kim, [a,b] and John P. Baltrus [a]

Cobalt is critical to energy-relevant technologies, and demand for cobalt will increase significantly with growing global adoption of renewables. However, supply chain stability is threatened by economic and geopolitical factors, incentivizing domestic cobalt production from alternative resources such as coal, coal utilization byproducts (e.g., ash, acid mine drainage) and electronic waste. Rapid, inexpensive, and portable characterization techniques are needed to reduce production costs associated with cobalt prospecting and process monitoring. In this research, we develop a compact, portable fiber optic luminescent probe for cobalt using phosphorus and nitrogen co-doped carbon dots as the sensing material. The carbon dot emission overlaps well with the cobalt absorption band at ~510 nm, leading to a selective decrease in emission as a function of cobalt concentration. The system responds nearly instantly to the presence of cobalt, with detection limits of 0.7 and 3.5 ppm in water and pH 1.68 buffer, respectively, providing comparable performance to a commercial spectrometer at a significantly lower cost. Moreover, the sensor is selective for cobalt in the presence of 13 of the most common metal ions encountered in coal utilization byproducts and is responsive to cobalt when spiked into an acid mine drainage leachate sample, highlighting the sensor's potential for real-world deployment in challenging matrices. In addition, integrating carbon dots with a filter paper substrate produced 'test strip' sensors that exhibited a selective and sensitive visual response to cobalt using a handheld UV lamp. Taken together, the sensing system represents a significant step in the development of low-cost practical sensors for high-value metals in complex streams.

Introduction

Cobalt is a crucial element for a range of applications[1] and is particularly important in the renewable energy sector, as it is a key component in lithium ion batteries used for electric vehicles[2] and is a major constituent of fuel cell cathodes.[3] As a result, demand for cobalt is expected to increase significantly in the coming decades.[4] Meanwhile, over half of global cobalt production occurs within a single country, the Democratic Republic of the Congo,[5] creating potential supply chain instabilities.[6] Economic factors are thus motivating policymakers to pursue cobalt production from domestic resources including electronic waste,[7, 8] seabed mining,[9] industrial refuse,[10, 11] and coal utilization byproducts such as acid mine drainage (and treatment solids),[12-14] fly ash,[15] and coal tailings.[16] The production of metals from alternative resources necessitates the development of characterization techniques that are inexpensive, portable, sensitive, and selective, and which can be used in the field to prospect for cobalt-rich sources and to monitor the efficiency and effectiveness of downstream processing steps[14] in which cobalt is extracted.[17]

Luminescence-based sensing techniques are attractive because they can offer significantly higher sensitivity than portable technologies such as handheld X-ray fluorescence (XRF) and laser-induced breakdown spectroscopy (LIBS) systems, are significantly less expensive than inductively-coupled plasma mass spectrometers (ICP-MS), and can be designed for portability, enabling field deployment.[18] Although reports of luminescent sensors for cobalt are relatively limited, several different material classes have been evaluated for Co detection, including metal-organic frameworks,[19-22] metal nanoparticles,[23-27] quantum dots,[28-30] organic molecules,[31-37] silicon nanomaterials,[38] polymers,[39] metal complexes,[40] and graphene/carbon quantum dots.[41-53] However, many of the sensors are not suitable for deployment in low pH environments[19, 26, 36, 40, 44, 49, 54-57] or aqueous systems,[22, 32, 40] suffer from cross-sensitivity with other metals,[28, 39, 41, 43, 53] and/or require a long or tedious synthetic approach.[21, 35, 37] Moreover, these luminescent sensors for cobalt have not been evaluated on low-cost, portable platforms that would be required for real-time process monitoring or cobalt prospecting, and often aren't tested in conditions relevant for coal utilizaiton byproduct streams. Thus, both material and instrument design are essential for lowering the characterization costs associated with metals production.

In this work, we integrate a carbon dot-based cobalt sensor with a lab-built fiber optic luminescent spectrometer that is

[a] National Energy Technology Laboratory, 626 Cochrans Mill Road, Pittsburgh, Pennsylvania 15236, United States.
[b] NETL Support Contractor, 626 Cochrans Mill Road, Pittsburgh, Pennsylvania 15236, United States
[c] *Scott.Crawford@netl.doe.gov

Electronic Supplementary Information (ESI) available: [details of any supplementary information available should be included here]. See DOI: 10.1039/x0xx00000x

both inexpensive (~$20,000), lightweight, and portable. Carbon dots were selected for studies using a portable sensor due to their stability at high ionic strength and low pH,[45, 58] tunable emission properties,[59-63] low cost,[64] and ease-of-synthesis.[47, 52] The carbon dots were synthesized by heating sucrose and urea through an acid-base reaction between phosphoric acid and ethylenediamine, creating phosphorus and nitrogen co-doped carbon dots. The material was characterized by X-ray photoelectron spectroscopy (XPS), absorption spectroscopy, transmission electron microscopy (TEM), and Fourier transform infrared spectroscopy (FTIR), and the luminescent properties and sensing response were evaluated on a commercial spectrometer. Then, the carbon dots were integrated with a slightly modified portable fiber optic sensor reported previously,[17, 65] demonstrating the ability to rapidly and selectively detect cobalt in neutral and acidic conditions. Importantly, the luminescent response was unique to cobalt, and the sensor performance was not significantly impacted by the presence of the most common metals in coal utilization byproduct streams (e.g., Al, Fe, Ca, Mn, Na). Moreover, the sensor responded to cobalt additions almost instantaneously, with low part-per-million detection limits, even in acidic conditions or in the presence of high salinity and/or elevated temperatures, and was also analyzed in a real fly ash leachate matrix. Taken together, these results represent a key step in the development of a portable luminescent cobalt sensor, a crucial need for low-cost cobalt production from domestic resources.

Experimental

Materials and Methods. Urea (≥98%), o-phosphoric acid (85%), potassium chloride (certified ACS), sulfuric acid (certified ACS) and pH 1.68 buffer (potassium tetroxalate dihydrate, Orion™) were purchased from Thermo Fisher Scientific (Whaltham, MA). Cobalt (II) nitrate hexahydrate (99+%), aluminum (III) nitrate nonahydrate (99+%), and iron (III) nitrate nonahydrate (99+%) were purchased from Acros Organics (Geel, Belgium). Ethylenediamine (≥99%), sucrose (≥99.5%), cerium (III) nitrate hexahydrate (99.99%), quinine sulfate, ethylenediaminetetraacetic acid disodium salt dihydrate (EDTA, 99.0-101.0%), neodymium (III) nitrate hexahydrate (99.9%), iron (II) sulfate heptahydrate (ACS reagent, ≥99.0%), sodium chloride (ACS reagent grade), calcium chloride (anhydrous), copper (II) nitrate trihydrate (99-104%), zinc nitrate hexahydrate (99.999%), and manganese (II) nitrate tetrahydrate (≥97.0%) were purchased from Sigma Aldrich (St. Louis, MO). Magnesium nitrate hexahydrate (ACS, 99.8-102.0%) and nickel (II) nitrate hexahydrate (98%) were purchased from Alfa Aesar (Haverhill, MA). De-ionized water (purity of 18.2 MW-cm, Barnstead EASYpure LF system) was used for all syntheses and measurements.

Synthesis of Carbon Dots. Carbon dots were synthesized by modifying a previously published protocol.[47] 0.15 g of sucrose and 0.05 g of urea were added to a 20 mL glass vial. 2 mL of concentrated phosphoric acid was added to the vial, and the vial was sonicated for 30 minutes to disperse the reactants in the phosphoric acid. 3 mL of ethylenediamine was rapidly added to the vial in a fume hood, and the vial was gently swirled for 3 seconds, and a rapid reaction between the acid and base ensued (*Caution: the acid/base reaction produces rapid localized heating. The reaction should be conducted in a fume hood and appropriate personal protective equipment should be worn)*. Once the vial cooled to room temperature, water was slowly added followed by gentle sonication. The resulting cloudy, brown-colored mixture was then diluted to 10 mL in water, sonicated and vortexed for 1 minute, and was then centrifuged for 10 minutes at 6500 rcf using a Beckman Coulter Allegra 64R centrifuge to remove larger species in solution. The transparent red-brown supernatant was then passed through a 0.45 µm PTFE Millex syringe filter (Merck, Kenilworth, NJ) and was dried overnight in an evaporating dish. Stock solutions were prepared by dissolving 4 mg of powder into 10 mL of water, which was stored at 4 °C until use.

Transmission Electron Microscopy (TEM). TEM characterization was performed on a Hitachi H9500 Environmental TEM with an accelerating voltage of 300 kV (NanoScale Fabrication and Characterization Facility, Petersen Institute of NanoScience and Engineering, Pittsburgh, PA), equipped with a Gatan Orius camera. A 0.4 mg/mL sample of carbon dots was diluted in deionized water until the color was a light brown (~1:50 dilution) and was dropcast onto an ultrathin carbon-coated holey TEM grid (Ted Pella, Inc.).

Fourier Transform Infrared Spectroscopy (FTIR). Attenuated Total Reflectance-Fourier Transform Infrared Spectroscopy (ATR-FTIR) spectroscopy was used to analyze changes to functional groups on carbon dots with and without cobalt exposure. Infrared spectra of samples were collected with a Vertex 70 (Bruker) Fourier transform infrared (FT-IR) spectrometer and GladiATR (Pike technologies) diamond ATR accessory. Samples were prepared by drop-casting and drying 100 µL of carbon dots onto a glass slide. In one sample, 50 µL of 0.1 M $Co(NO_3)_2$ was added to the carbon dots and gently mixed with a pipette. The samples were allowed to dry in air. A glass slide was used to record the background spectra and was subtracted from the spectra for each sample.

X-ray Photoelectron Spectroscopy (XPS). Samples were prepared on a glass slide using the same conditions described in the FTIR characterization section. XPS spectra of carbon dots with and without cobalt exposure were acquired with a ULVAC-PHI Versa Probe III instrument using a focused (200 µm) monochromatized Al Kα X-ray source (1486.6 eV) and dual charge neutralization. The electron and ion neutralization current densities were set at 22 nA/mm^2 and 250 pA/mm^2, respectively. A pass energy of 55.0 eV was used for all high-resolution scans, whereas a pass energy of 140 eV was used for the collection of survey spectra. High resolution spectra were charge corrected using C1s = 284.8 eV as a reference energy.

Photoluminescence Characterization using a Commercial System. Initial photoluminescent studies of the carbon dots were conducted on a Horiba Jobin-Yvon Fluorolog 3 equipped with FluorEssence software and a 450 W xenon lamp. Excitation and emission slits were set to 5 nm, with a 0.1 s integration time. A 400 nm cut-off filter (Edmund Optics) was used to block

excitation light from reaching the detector. Quartz cuvettes (Thorlabs, Inc) were used for all measurements. In a typical experiment, 15 µL of the filtered carbon dots were added to 2 mL of water (for studies under acidic conditions, 15 µL of carbon dots were added to a cuvette containing 1 mL of pH 1.68 buffer and 1 mL of water). For limit of detection studies, 0.1 M $Co(NO_3)_2$ was titrated into the carbon dot solution, and the Fluorolog was programmed to measure intensity at the emission maximum (500 nm) every 0.1 second for 10 seconds, producing 100 data points for each concentration level of cobalt tested. The intensity (I) at each concentration was averaged and then divided by the average intensity when no cobalt was added (I_0). A calibration curve using the Stern-Volmer relationship (1) was then plotted against the concentration (Q):

(1) $$(\frac{I}{I_0} - 1) = m[Q]$$

The slope "m" of the plot was used as an estimate of sensitivity. To estimate the noise, each data point collected at the lowest cobalt concentration tested was divided by the average intensity of the sample with no cobalt added (e.g., I_0). The standard deviation (s) was then calculated for these numbers. The limit of detection (LOD) was then calculated using (2):[66]

(2) $$LOD = 3 * \frac{s}{m}$$

The limit of quantification (LOQ) was then estimated using (3):[66]

(3) $$LOQ = 10 * \frac{s}{m}$$

For selectivity studies, the emission spectrum of the carbon dots in water was first collected. Then, 10 µL of each 0.1 M metal ion solution being tested was added, and the sample was capped and gently shaken by hand before collecting the emission spectrum. Finally, 10 µL of a 0.1 M $Co(NO_3)_2$ was added, the vial was again shaken by hand, and the emission spectrum was collected. This experiment was repeated at least 3 times for each metal ion tested.

Quantum Yield Determination. The quantum yield of the carbon dots was estimated relative to quinine sulfate in 0.1 M sulfuric acid.[67] The relative quantum yield (Φ) (was estimated using (4):

(4) $$\frac{\Phi}{\Phi_r} = \left[\frac{A_r(\lambda_r)}{A_x(\lambda_x)}\right]\left[\frac{I(\lambda_r)}{I(\lambda_x)}\right]\left[\frac{n_x^2}{n_r^2}\right]\left[\frac{D_x}{D_r}\right]$$

where *A* is the absorbance at the excitation wavelength (λ), *I* is the intensity of the excitation light at the same wavelength, *n* is the refractive index (1.33 for both the reference and standard), and *D* is the integrated luminescence intensity (390-700 nm). The subscripts '*x*' and '*r*' refer to the sample and reference, respectively. The reference quantum yield Φ_r from quinine sulfate was 0.54. Optically dilute conditions (absorbance < 0.2 at 365 nm) were used for all measurements (7 quinine sulfate standards and 5 independently synthesized batches of carbon dots).

Absorption Spectroscopy Characterization. Absorption spectra were collected on a Perkin-Elmer Lamba 1050 spectrometer. 15 µL of carbon dots were added to quartz cuvettes (Thorlabs, Inc.) containing 2 mL of water or 2 mL of pH 1.68 buffer, and spectra were collected before and after additions of 0.1 M cobalt nitrate. Absorption spectra were also collected for a 0.05 M cobalt nitrate solution. To probe the impact of other metals, dilute carbon dot solutions (absorbance ~0.05 at 360 nm) were prepared and analyzed after exposure to 0.5 mM concentrations of different metals.

Sensing Experiments Using a Portable Spectrometer. In order to evaluate the feasibility of developing low-cost, portable cobalt sensors using carbon dots, the sensing performance of the carbon dots were analyzed using a custom-built, portable fiber optic spectrometer that has been described elsewhere,[17, 65] with minor modifications. A schematic for the sensor is included in the supporting information (Figure S1). A mounted 365 nm LED (Thorlabs, M365LP1, 1350 mW, with a Thorlabs DC2100 LED Driver) was equipped with a Thorlabs LA4025 lens and a 240-395 nm bandpass filter (Thorlabs FGUV5M). Light from the LED was transmitted into the 9-fiber arm of a Y-shaped bifurcated optical fiber cable (Thorlabs BF19Y2HS02, solarization-resistant 19–200 µm 0.22NA fiber bifurcated cable bundle). The 19-fiber end of the bifurcated cable was immersed in a 20 mL amber vial containing the carbon dot solution. Emission from the sample was passed through the 10-fiber the bifurcated cable branch, was transmitted through an aspheric lens (Thorlabs, C220TME-A), a 400 nm longpass filter (Thorlabs, FELH0400), and then through a second aspheric lens (Thorlabs, C220TME-A), where the emitted light was detected by an OceanOptics QEPRO spectrometer with OceanView software. An integration scan of 3 s was used, and 3 scans were averaged during each period of data collection. In all cases, a "dark" spectrum, collected without LED illumination, was subtracted from all spectra.

In a typical experiment, a 150 µL aliquot of the filtered carbon dots was added to an amber vial containing 19.85 mL of water (for studies in acidic conditions, the carbon dots were added to a pH 1.68 buffer diluted by an equal volume of water). For selectivity studies, the carbon dot emission profile was first collected, and then 100 µL of a 0.1 M metal ion solution was added. After gentle mixing with a pipette, the emission spectrum was again collected. Finally, 100 µL of a 0.1 M $Co(NO_3)_2$ was added, the sample was again mixed, and the emission spectrum was collected. This process was repeated at least 3 times for all metals studied. For limits of detection studies, a strip chart was created using OceanView that monitored intensity at the emission maximum (500 nm) after each $Co(NO_3)_2$ addition to the carbon dot solution. At least 7 data points were collected at each $Co(NO_3)_2$ concentration level, and at least 7 data points were used for the calibration curves used to estimate limits of detection.

Concentration Studies. In order to optimize the concentration of carbon dots used for cobalt detection, various volumes of the 0.4 mg/mL stock solution were added to an amber vial, and the carbon dots were diluted to 10 mL of total volume. The portable spectrometer was used to analyze carbon dot emission before and after the addition of 50 µL of a 0.1 M $Co(NO_3)_2$ solution. At least three independent trials were conducted at each carbon dot concentration level.

Photostability Studies. An amber vial containing a stir bar and 75 µL of the 0.4 mg/mL carbon dot stock solution diluted to 10 mL of water was placed on a hot/stir plate with a stirring rate of 300 rpm. The portable spectrometer was used to analyze the

carbon dot emission as a function of time over the course of 7 hours. This process was repeated on three different carbon dot samples.

Stability Tests. Four samples containing 75 µL of the 0.4 mg/mL carbon dot stock solution were diluted to 10 mL of water and were stored at room temperature in amber vials. The luminescent are was measured on different days over the course of 1 month using the portable spectrometer.

Salinity Studies. The sensor performance of the carbon dots as s function of ionic strength was evaluated by dispersing 75 µL of the 0.4 mg/mL carbon dot stock solution in 10 mL of different concentrations of sodium chloride (from 0 to 2 M). The portable spectrometer was used to analyze carbon dot emission before and after the addition of 50 µL of a 0.1 M $Co(NO_3)_2$ solution. At least three independent trials were conducted at each NaCl concentration.

Temperature Studies. An amber vial containing a stir bar and 75 µL of the 0.4 mg/mL carbon dot stock solution diluted to 10 mL of water was placed on a hot/stir plate equipped with a temperature probe. The stir rate was set to 300 rpm, and the temperature probe was placed into the carbon dot solution. The portable spectrometer was used to analyze the carbon dot emission before and after the addition of 50 µL of a 0.1 M $Co(NO_3)_2$ solution at various temperatures. At least three independent trials were conducted at each temperature point.

Process Stream Characterization. A sample of acid mine drainage leachate was collected, and its metal content was characterized by inductively-coupled plasma mass spectrometry (ICP-MS).

Cobalt Sensing 'Test Strips.' Test paper for rapid, visual cobalt detection was prepared by slowly dropcasting 1 mL of filtered carbon dots diluted 1:6 in water onto a 90 mm diameter ashless filter paper (No. 42, Whatman International LTD, Maidstone, UK) substrate. The carbon dot-soaked paper was then dried for ~5 minutes in a laboratory oven set at 90 °C. Upon drying, the paper was cut into ~0.75 in by 0.75 in squares. A 0.1 M $Co(NO_3)_2$ stock solution was prepared, and used to make 1 mL of various cobalt solutions ranging in concentration from 0.1 mM to 0.1 M. Carbon dot-coated paper strips were fully immersed into the cobalt solutions of different concentrations using tweezers for ~10 seconds. The strips were then allowed to dry in air, and were photographed using a cell phone camera (iPhone 8, Apple Inc.) under a 6 W 365 nm UV lamp (Antalytik Jena, UVGL-55, Jena, Germany). The same lamp and camera were used for all photography under UV light.

Results and Discussion

Material science is crucial for the development of high-performance materials for the luminescence-based detection of cobalt. The ideal material should exhibit an emission response that is unique to cobalt, with high sensitivity across a wide concentration range. Moreover, the sensing material should be stable and responsive under acidic conditions, which would enable deployment in the low pH conditions typically encountered when processing coal utilization byproducts and electronic waste leachates. Other considerations, such as ease-of-synthesis and material costs, are also important for the development of inexpensive sensors.

A common mechanism for the selective detection of cobalt is to develop sensors with emission bands that overlap with cobalt's absorption band, leading to a cobalt concentration-dependent quenching of the sensor's emission.[22, 46, 47, 58] Thus, a modification was made to a previously described synthesis of cobalt-responsive carbon dots (λ_{EM} = 450 nm)[47] by adding urea, a common nitrogen source for the synthesis of cobalt-sensitive carbon dots,[46, 52] to increase nitrogen doping. Increased nitrogen doping should, in turn, produce a redshift in the emission maximum,[62] leading to better overlap with cobalt absorbance (~510 nm, **Figure S2**).[58] The synthetic approach used here requires inexpensive materials (urea, sucrose, ethylene diamine and phosphoric acid), is rapid (~5 minute reaction time), and relies on localized heating from the acid-base reaction between phosphoric acid and ethylenediamine, avoiding the use of ovens or other external heating sources. The acid-base reaction also leads to both phosphorus and nitrogen doping within the carbon dots, both of which contribute to a red-shift in the carbon dot emission profile to better overlap with cobalt absorption. Moreover, the phosphoric acid reaction also produces oxidized phosphorus groups that can aid in metal ion chelation, as evidenced by FTIR characterization (along with nitrogen and oxygen, *vide infra*).

Physical Characterization. The purified carbon dots were characterized by a range of techniques, including TEM, XPS, FTIR, absorption spectroscopy, and photoluminescence spectroscopy. Imaging by TEM revealed small pseudospherical nanoparticles with an average diameter of 5 ± 1 nm (**Figure S3**). XPS analyses taken before and after cobalt exposure reveal the presence of all expected elements: carbon, nitrogen, phosphorus, and oxygen (**Figure S4**). Cobalt signal was observed for the cobalt-exposed sample, and evidence of oxidation was observed in the oxygen and nitrogen high-resolution spectra, consistent with chelation by oxygen and nitrogen-containing functional groups (**Figure S5**). Surface elemental analysis using the high-resolution XPS peaks indicated that the carbon dots are approximately 56% (atomic %) carbon, 21% oxygen, 21% nitrogen, and 2% phosphorus. FTIR analysis revealed the presence of oxidized phosphorus groups (P-OH at ~2500-2700 cm^{-1} and 950 cm^{-1}, P=O at 1150 cm^{-1},and P-OR at ~1050 cm^{-1}), carbonyl groups (~1640 cm^{-1}), imines (1560 cm^{-1}), as well as amino and hydroxyl functionalities (~3170 cm^{-1}, 3330 cm^{-1}, and 3650 cm^{-1}) consistent with reports on similar carbon dot systems.[47] Upon exposure to Co^{2+}, the transmission intensity generally increases, with particular broadening and weaking of the amino, hydroxyl, and carboxylate peaks, suggesting metal ion chelation (**Figure S6**).[32, 54, 68]

Photoluminescence Characterization. Figure 1 illustrates visual changes in the carbon dot optical properties as a function of cobalt concentration under a 365 nm UV lamp, revealing blue-green emission that was quenched by cobalt additions (**Video S1),** with a corresponding darkening of the carbon dot solution to a red-brown with increasing cobalt concentration, suggesting the formation of a complex.[48, 51] The luminescent and sensing properties of the carbon dots were evaluated more

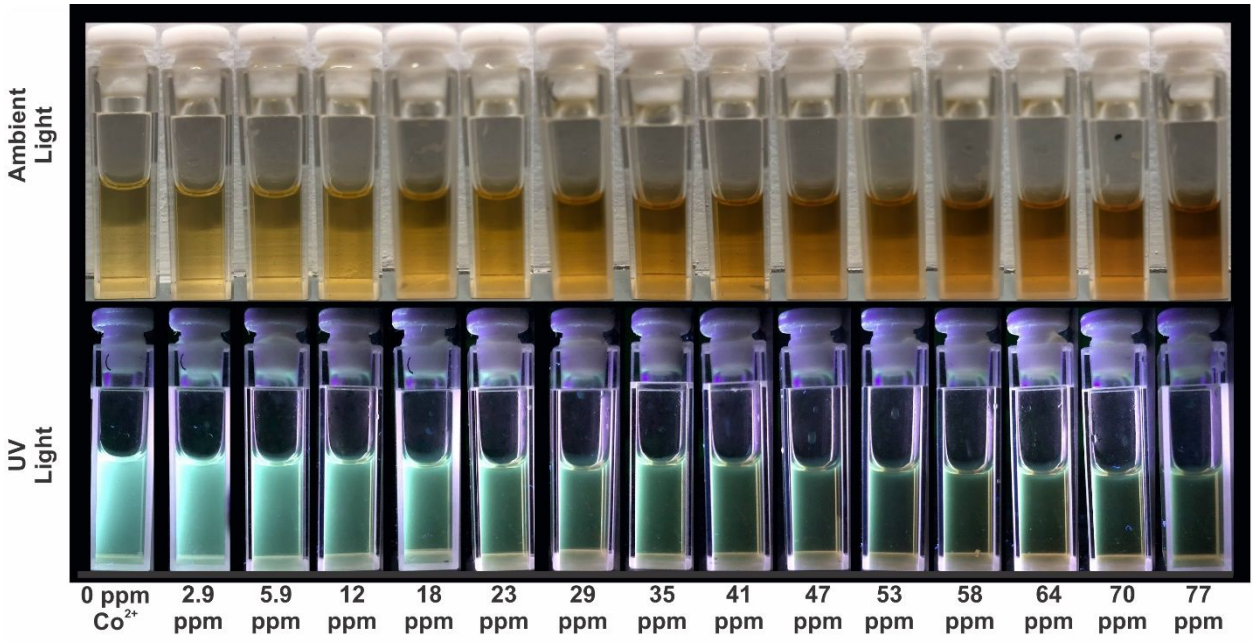

Figure 1. Digital photographs of concentrated carbon dots in water under ambient light (top) and 365 nm light (bottom) in the presence of increasing cobalt concentration.

quantitatively using a commercial Fluorolog 3 system. The relative quantum yield, estimated by comparison to quinine sulfate standards, was 3.3% ± 0.3% for 5 synthetic batches. In order to optimize the concentration of carbon dots used to detect cobalt, experiments were conducted in which the emission properties were evaluated at different carbon dot concentrations before and after the addition of cobalt (**Figure S7**). Based upon these experiments, a concentration of 0.3 mg/L was used for all luminescent sensing studies. The photostability of the carbon dots was also analyzed by measuring luminescence intensity under constant irradiation over the course of 7 hours, and these tests revealed only a modest decrease in emission (**Figure S8**). The stability of the carbon dots as a function of storage time was also evaluated by characterizing the luminescent properties of the carbon dots over the course of one month (**Figure S9)**, which also indicated excellent stability.

Titrations designed to estimate limits of detection (LODs) were conducted in both deionized water (**Figure S10**) and in pH 1.68 buffer (to simulate acidic conditions encountered in coal ash leachates). In deionized water, an LOD of 0.15 ± 0.03 ppm (LOQ = 0.51 ± 0.09 ppm) was achieved, with a linear range of ~0 to 20 ppm Co. The sensitivity was poorer in pH 1.68 media, with an LOD of 8 ± 1 ppm (LOQ: 21 ± 3 ppm), with a longer linear dynamic range of 0 to 200 ppm (**Figure S11**). Differences in sensitivity due to pH may be due to competition for binding sites between protons and cobalt: in deionized water, the Stern-Volmer profile was exponential in nature, indicating both dynamic and static quenching, whereas a plateau was observed in acidic media, indicating inaccessible luminophores that may be prevented from chelating cobalt due to proton binding (Figure S6B, S7B).[69] Moreover, the excitation profiles responded differently as a function of pH: in deionized water, an excitation peak centered at 365 nm gradually redshifted upon cobalt addition, whereas in pH 1.68 buffer, the excitation peak centered at 385 nm did not shift as a function of cobalt concentration (**Figure S12).** Differences in the absorbance spectrum were also evident: in deionized water, the carbon dots exhibited an absorption band at 365 nm that became more intense and redshifted with increasing Co(II) concentration (**Figure S13**). In pH 1.68 buffer, no peak shifts were observed, while an increase in absorbance was most prominent towards the deep UV (e.g., 250 nm to 300 nm). Significantly, in both cases the LOD was near or below the Co concentrations found in coal and utilization byproducts such as ash.[70] With sensitivity estimates in hand, selectivity studies were conducted in which the luminescent of the carbon dots was measured before and after the addition of 0.5 mM of 13 of the most common metals encountered in coal-based samples, and again after the addition of 0.5 mM cobalt. In all cases, drastic quenching (I_0/I = ~0.2) was observed only after the addition of cobalt, indicating a highly selective sensor for cobalt (**Figure S14**).

Characterization using a portable sensor. A key advantage of luminescence-based characterization techniques versus methods such as ICP-MS is that portable spectrometers can be developed for facile transportation to field sites for metal prospecting or between labs for the characterization of downstream processing steps.[17, 71] The use of less expensive and/or miniaturized equipment relative to commercial instrumentation can lead to trade-offs in sensing performance, however. Therefore, to determine whether the carbon dot based cobalt sensor could be practical for portable sensing applications, the cobalt sensor's performance was evaluated using a custom-built, portable, fiber optic-based spectrometer

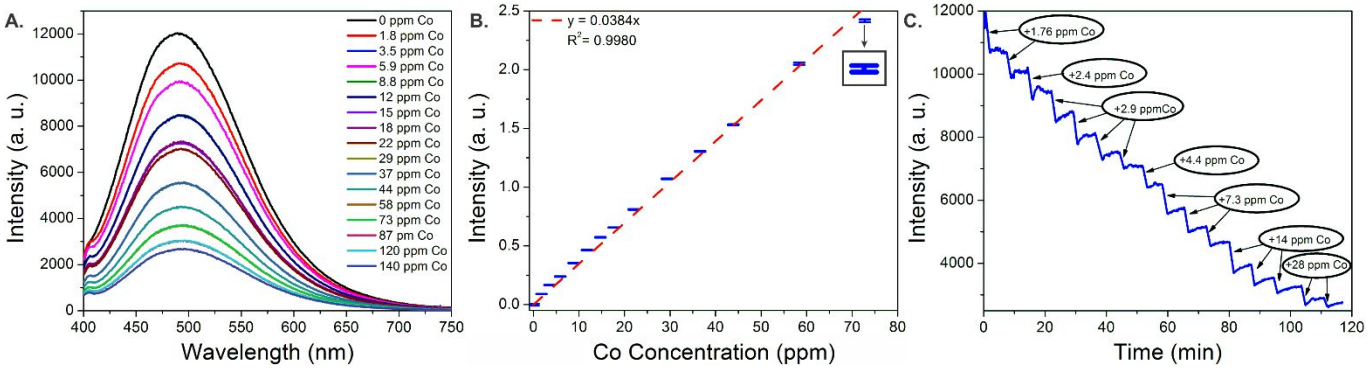

Figure 2. Emission spectra of carbon dots in the presence of increasing cobalt concentration (A), calibration curve used to estimate limits of detection, where error bars (one of which is magnified in the inset for clarity) denote the standard deviation of at least 7 independent measurements (B), and the response of the sensor as a function of time following various cobalt additions (C), recorded using a portable fiber optic probe.

(**Figure S1**). The probe was fist monitored for its sensitivity for cobalt in water. As illustrated in **Figure 2**, the sensor was responsive to low-ppm additions of Co^{2+}, with a linear range up to ~80 ppm Co. Changes in luminescent signal in response to Co^{2+} additions were nearly instantaneous, enabling rapid characterization. A detection limit of 0.6 ± 0.1 ppm (LOQ: 2.0 ± 0.4 ppm) was estimated across three independent trials.

Similarly, the sensitivity of the carbon dots was evaluated with the portable sensor in pH 1.68 buffer. Similar to the results obtained using the Fluorolog, a decrease in sensitivity was observed in an acidic environment. However, the portable sensor notably outperformed the commercial fluorimeter, attaining an LOD of 3.5 ± 0.5 ppm (LOQ: 12 ± 2 ppm) across three trials (**Figure 3**). Moreover, in both deionized water and acid, a significantly larger linear dynamic range was achieved using the portable sensor, an important consideration for practical deployment. Improvements in linear dynamic ranges have been reported in other fluorescence-based sensors using lower powered excitation sources.[72]

Selectivity studies again revealed that cobalt produced a unique quenching response relative to 13 of some of the most common metals encountered in coal utilization byproducts (**Figure 4**), though the changes in luminescence intensity were less drastic upon cobalt addition relative to the results observed using the Fluorolog 3 system. In general, the presence of competing metal ions at concentrations equal to the added cobalt did not significantly interfere with cobalt-mediated luminescence quenching. Moreover, of the 13 metals tested, cobalt uniquely produced a significant colorimetric response, leading to increased absorption in the UV (**Figure 4C**) that could easily be observed visually (**Figure 4D**), suggesting the carbon dots preferentially form a complex with cobalt. Of course, cobalt-containing process streams are often quite complex, with high ionic strength, low pH, and multiple metal ions. To further analyze the impact of matrix effects, the carbon dot's response to cobalt was evaluated as a functional of salinity using different concentrations of sodium chloride (**Figure S15**) and at elevated temperatures (**Figure S16**). The sensor performance was not significantly impacted as a function of ionic strength (from 0 to 2 M NaCl), and was fairly tolerant to moderate temperature increases up to ~70 °C. Finally, a cobalt titration was carried out in an actual fly ash leachate matrix and the response of the sensor was evaluated. As expected, the sensitivity of the system was hampered by the low pH (1.5) and high concentrations of competing metal ions (**Table S1**). A linear quenching profile was observed upon the addition of increasing concentrations of cobalt (**Figure S17**), indicating that the senor

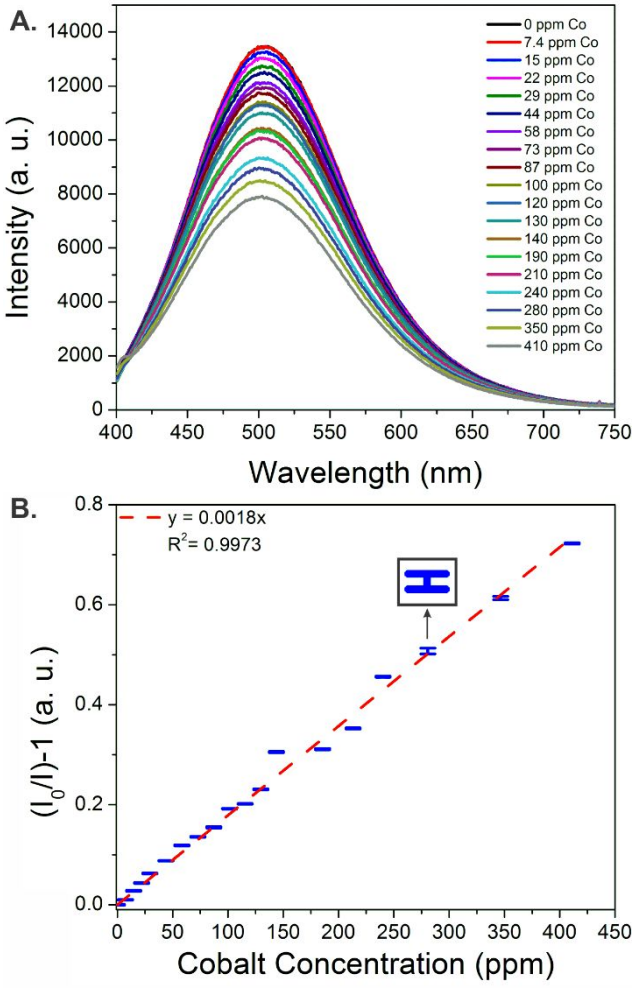

Figure 3. Representative emission spectra (A) and calibration curve (B) of the carbon dot sensor in the presence of increasing cobalt concentration in pH 1.68 buffer, recorded using the portable fiber optic probe. Error bars, one of which is magnified in the inset for clarity, represent the standard deviation of at least 7 measurements for each data point.

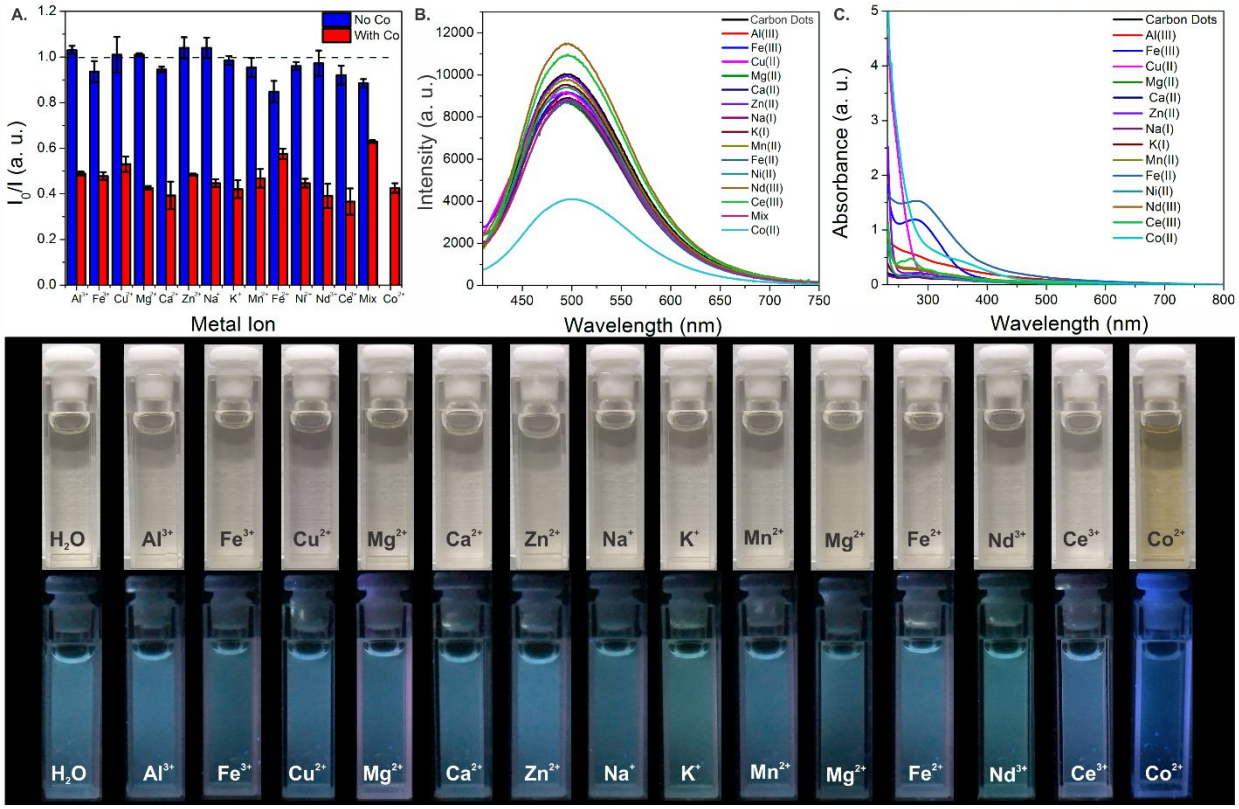

Figure 4. A. Changes in the carbon dot emission peak area after the addition of 0.5 mM of different metals (blue) and after the subsequent addition of 0.5 mM cobalt (red). B. Representative emission spectra of the carbon dots after the addition of different metals, measured using the portable fiber optic spectrometer. C. Normalized absorption profile of dilute carbon dot solutions exposed to each metal solution. D. Photographs of dilute carbon dot solutions exposed to 0.5 mM of different metals under ambient and UV light.

should be capable of deployment in real-world streams provided a suitable matrix is used when creating a calibration curve.

Mechanistic Summary. A common method for designing sensitive luminescent sensors for cobalt is to have overlap between the sensor emission band and the cobalt absorption band at ~510 nm. Moreover, the ideal sensor should selectively interact with cobalt in the presence of other metal ions. Figure S2 indicates that there is indeed significant overlap of carbon dot emission with cobalt absorption. Figure 4 further reveals a colorimetric response that is unique to cobalt, as the carbon dot solution turns from a faint yellow-brown to a deep red-brown, consistent with the formation of a complex with cobalt, whereas other metals do not produce significant changes.[48, 51] This stark response to cobalt suggests a high affinity between cobalt and the sensor, consistent with FTIR and XPS analysis, which both indicate chelation of cobalt by multiple functional groups, including amines, carboxylates, and phosphates (Figures S5 and S6). The importance of cobalt chelation to the quenching mechanism is further elucidated by reversibility studies, in which the chelating agent EDTA is added to the carbon dots following cobalt exposure. In these experiments, luminescence intensity is partially restored upon EDTA addition, coupled with a decrease in UV absorption and a corresponding lightening of color (**Figure S18)**. The exponential nature of the Stern-Volmer profile in water (**Figure S10**) further suggests multiple quenching processes occur simultaneously upon cobalt addition, and this quenching is influenced in part by pH; at pH 1.68 (**Figure S11**), a plateau is observed, indicating inaccessible luminophores. The lack of significant colorimetric changes in response to cobalt addition under acidic conditions suggest that protonation of carbon dot functional groups may hinder cobalt chelation. More specific insights into the exact binding environment may be aided by computational modelling.[73-76]

Development of 'Test Strip' Sensors for Cobalt Detection. A common strategy for minimizing the cost of qualitative luminescent sensors is to fabricate 'test strips,' in which the sensing material is deployed as a thin film on a substrate,[77] such as filter paper,[19, 38, 48, 78, 79] fabric,[80] glass,[81, 82] or polymer,[83] among others. The sensor can then be integrated with a simple light source for naked eye detection of analytes of interest, or even used in tandem with smart phone spectrometers for more quantitative analysis, providing a low-cost and portable detection platform.[84] As a proof-of-concept, filter paper test strips for cobalt were prepared by incubating filter paper in a diluted carbon dot solution (full details in the experimental section), followed by drying in a laboratory oven. The test strips were then exposed to various concentrations of $Co(NO_3)_2$. The test strips exhibited bright emission under UV excitation prior to Co^{2+} exposure, and this emission was quenched with

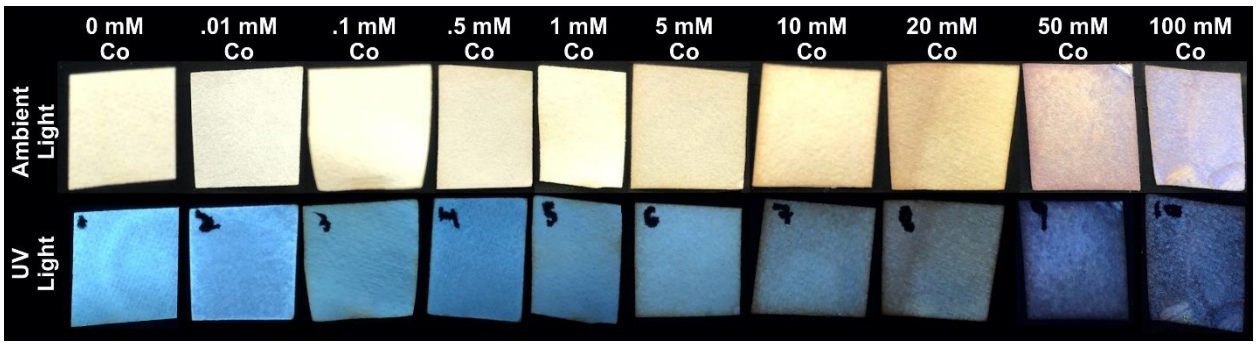

Figure 5. Carbon-dot coated test strips exposed to increasing concentrations of Co^{2+} under ambient light (top) and 365 nm light (bottom). Emission quenching is observed as a function of cobalt concentration.

increasing Co^{2+} concentration. Analogous changes in the test strip color were observed under ambient light (**Figure 5**).

The selectivity of the filter paper cobalt sensors was probed by exposing paper strips to 10 mM concentrations of the same metal ions shown in Figure 4. Of the metals tested, only cobalt produced significant quenching that could be observed with the naked eye (Figure 6) under UV light. The 'test strips' were further challenged by conducting studies in which one test strip was exposed to a solution containing 10 mM of all metals (e.g. Al(III), Fe(II), Cu(II), Mg(II), Ca(II), Zn(II), Na(I), K(I), Mn(II), Fe(III), Ni(II), Nd(III), and Ce(III)), and another test strip was exposed to the same solution with 10 mM Co^{2+} also added. Significantly more quenching was observed after cobalt addition (Figure S19), highlighting the selectivity of the test strips for cobalt. In addition, test strips were evaluated in a real acid mine drainage sample (Table S2) spiked with different cobalt concentrations, and, even in this more complex matrix, a clear quenching response was again observed as a function of cobalt concentration (Figure S20). Compared with other carbon dot-based test strip sensors for cobalt,[38, 48, 79] the strips presented here exhibit a more distinct response to cobalt and/or have been evaluated under a wider range of environmentally-relevant conditions. These carbon dot-laden test strips provide another simplistic portable technique for qualitative cobalt analysis.

Conclusions

With global economic trends incentivizing increased domestic production of cobalt, high-performance, portable, and inexpensive sensing platforms are needed to characterize cobalt concentrations in the field and during downstream processing. Here, we demonstrate a portable sensing platform utilizing a carbon dot sensing material for the luminescence-based detection of cobalt. The carbon dot sensing material offers a number of advantages, including ease-of-synthesis, in which heat from an acid-base reaction circumvents long reaction times, external heating, and/or the use of synthesis ovens or microwaves. Moreover, these carbon dots exhibit excellent stability at low pH and high salinity, and high selectivity for cobalt over competing ions commonly found in metal-containing environmental streams such as acid mine drainage. Importantly, the sensing material's performance is benchmarked using a relatively inexpensive and fully portable fiber optic sensing platform that would be more relevant for process monitoring and/or prospecting applications. This sensing platform is capable of part-per-billion levels of cobalt detection with a linear range of nearly 100 ppm and is selective for cobalt against 13 of the most common metal ions encountered in coal byproduct streams. Moreover, the sensor is responsive to cobalt additions in challenging matrices, such as high salinity/low pH streams and in real acid mine drainage leachates. Importantly, the carbon dot sensing performance is

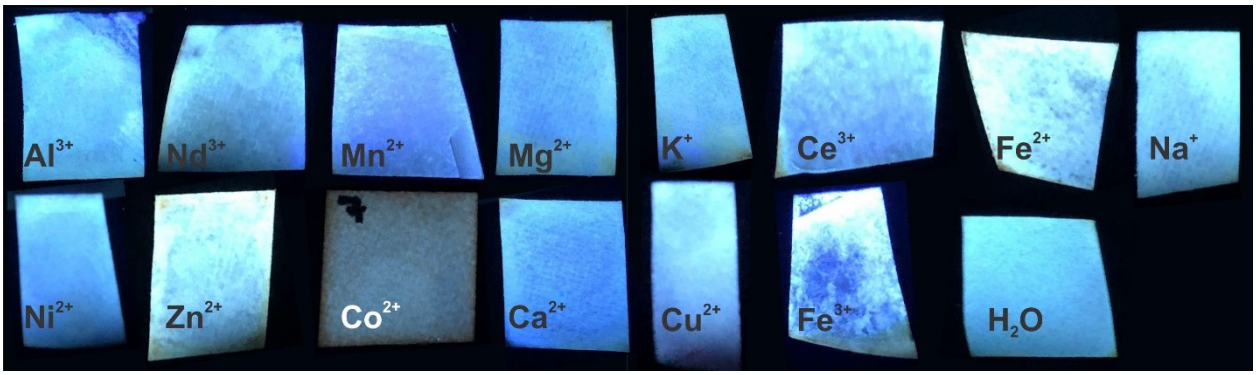

Figure 6. The carbon-dot coated test strips exposed to 10 mM concentrations of different metal ions commonly encountered in coal and its associated utilization byproduct streams under a 365 nm UV lamp. Only cobalt produces significant quenching

evaluated using both a commercial and portable system, and comparable performance is achieved using the less expensive system. The platform can be further simplified for qualitative cobalt sensing using filter paper test strips. Taken together, this work represents a step forward in the development of cobalt sensing technologies, a critical need for the energy sector that will become increasingly important in the coming decades.

Conflicts of interest

The authors declare no conflicts of interest.

Acknowledgements

The authors thank Drs. Christopher Matranga and Viet Pham for helpful conversations on carbon dot synthesis and characterization and Dr. Ward Burgess for assistance with process stream characterization. This project was funded by the United States Department of Energy, National Energy Technology Laboratory, in part, through a site support contract. Neither the United States Government nor any agency thereof, nor any of their employees, nor the support contractor, nor any of their employees, makes any warranty, express or implied, or assumes any legal liability or responsibility for the accuracy, completeness, or usefulness of any information, apparatus, product, or process disclosed, or represents that its use would not infringe privately owned rights. Reference herein to any specific commercial product, process, or service by trade name, trademark, manufacturer, or otherwise does not necessarily constitute or imply its endorsement, recommendation, or favoring by the United States Government or any agency thereof. The views and opinions of authors expressed herein do not necessarily state or reflect those of the United States Government or any agency thereof.

Notes and references

1 A. Tkaczyk, A. Bartl, A. Amato, V. Lapkovskis and M. Petranikova, *J. Phys. D: Appl. Phys.*, 2018, **51**, 203001.
2 G. A. Campbell, *Miner. Econ.*, 2020, **33**, 21-28.
3 N. A. Baharuddin, A. Muchtar and M. R. Somalu, *Int. J. Hydrog. Energy*, 2017, **42**, 9149-9155.
4 J. Baars, T. Domenech, R. Bleischwitz, H. E. Melin and O. Heidrich, *Nat. Sustain.*, 2021, **4**, 71-79.
5 M. L. Shengo, M.-B. Kime, M. P. Mambwe and T. K. Nyembo, *J. Sustain. Min.*, 2019, **18**, 226-246.
6 X. Fu, D. N. Beatty, G. G. Gaustad, G. Ceder, R. Roth, R. E. Kirchain, M. Bustamante, C. Babbitt and E. A. Olivetti, *Environ. Sci. Technol.*, 2020, **54**, 2985-2993.
7 M. K. Jha, A. Kumari, A. K. Jha, V. Kumar, J. Hait and B. D. Pandey, *Waste Manage.*, 2013, **33**, 1890-1897.
8 H. Gomaa, S. El-Safty, M. Shenashen, S. Kawada, H. Yamaguchi, M. Abdelmottaleb and M. Cheira, *ACS Sustain. Chem. Eng.*, 2018, **6**, 13813-13825.
9 J. R. Hein, T. A. Conrad and R. E. Dunham, *Marine Georesources and Geotechnol.*, 2009, **27**, 160-176.
10 A. Kadłubowicz, M. Janiszewska, M. Baraniak, G. Lota, K. Staszak and M. Regel-Rosocka, *J. Water Process Eng.*, 2021, **39**, 101754.
11 Z. Wiecka, M. Rzelewska-Piekut, R. Cierpiszewski, K. Staszak and M. Regel-Rosocka, *Catalysts*, 2020, **10**, 61.
12 B. C. Hedin, R. S. Hedin, R. C. Capo and B. W. Stewart, *International J. Coal Geol.*, 2020, **231**, 103610.
13 W. Zhang and R. Honaker, *Miner. Eng.*, 2020, **153**, 106382.
14 Q. Li and W. Zhang, *Resour. Conserv. Recycl.*, 2022, **180**, 106214.
15 T. Ju, S. Han, Y. Meng and J. Jiang, *ACS Sustain. Chem. Eng.*, 2021, **9**, 6894-6911.
16 W. Zhang and R. Honaker, *Fuel*, 2020, **267**, 117236.
17 J. C. Ahern, Z. L. Poole, J. Baltrus and P. R. Ohodnicki, *IEEE Sens. J.*, 2017, **17**, 2644-2648.
18 S. E. Crawford, J. E. Ellis, P. R. Ohodnicki and J. P. Baltrus, *ACS Appl. Mater. Interfaces*, 2021, **13**, 7268-7277.
19 K. Xing, R. Fan, X. Du, Y. Song, W. Chen, X. Zhou, X. Zheng, P. Wang and Y. Yang, *Sens. Actuators B*, 2018, **257**, 68-76.
20 Y.-H. Han, C.-B. Tian and S.-W. Du, *Dalton Trans.*, 2014, **43**, 11461-11464.
21 K. Xing, R. Fan, J. Wang, S. Zhang, K. Feng, X. Du, Y. Song, P. Wang and Y. Yang, *ACS Appl. Mater. Interfaces*, 2017, **9**, 19881-19893.
22 Z. Cui, X. Zhang, S. Liu, L. Zhou, W. Li and J. Zhang, *Inorg. Chem.*, 2018, **57**, 11463-11473.
23 C. Shao, S. Xiong, X. Cao, C. Zhang, T. Luo and G. Liu, *Microchem. J.*, 2021, **163**, 105922.
24 J. R. Lakkakula, D. Divakaran, M. Thakur, M. K. Kumawat and R. Srivastava, *Sens. Actuators B*, 2018, **262**, 270-281.
25 B. A. Lakshmi, J.-Y. Bae, J. H. An and S. Kim, *Microchim. Acta*, 2019, **186**, 1-11.
26 R.-X. Zhao, A.-Y. Liu, Q.-L. Wen, B.-C. Wu, J. Wang, Y.-L. Hu, Z.-F. Pu, J. Ling and Q. Cao, *Spectrochim Acta A Mol Biomol Spectrosc*, 2021, **254**, 119628.
27 K. Ngamdee, T. Tuntulani and W. Ngeontae, *Sens. Actuators B*, 2015, **216**, 150-158.
28 N. Mahapatra, S. Panja, A. Mandal and M. Halder, *J Mater Chem C*, 2014, **2**, 7373-7384.
29 S. Geng, S. M. Lin, Y. Shi, N. B. Li and H. Q. Luo, *Microchim. Acta*, 2017, **184**, 2533-2539.
30 W. Bian, J. Ma, Q. Liu, Y. Wei, Y. Li, C. Dong and S. Shuang, *Luminescence*, 2014, **29**, 151-157.
31 Z. Liu, W. Wang, H. Xu, L. Sheng, S. Chen, D. Huang and F. Sun, *Inorg. Chem. Commun.*, 2015, **62**, 19-23.
32 F. Fateh, A. Yildirim, A. A. Bhatti and M. Yilmaz, *J. Fluoresc.*, 2021, **31**, 1075-1083.
33 M. Zhu, W. Wang, J. Liu, R. Na, Z. Li and Y. Wang, *J. Mol. Liq.*, 2020, **303**, 112680.
34 L. Ji, C. Yang, H. Li, N. Yang, Y. Fu, L. Yang, Q. Wang and G. He, *Luminescence*, 2021, **36**, 4-10.
35 H. Liu, M. Li, Y. Zhang, H. Yang, Y. Yang, X. Xu, Z. Wang and S. Wang, *Spectrochim Acta A Mol Biomol Spectrosc*, 2021, **248**, 119213.
36 J. J. Celestina, P. Tharmaraj, C. Sheela and J. Shakina, *J. Lumin.*, 2021, **239**, 118359.
37 A. Pramanik, S. Amer, F. Grynszpan and M. Levine, *Chem. Commun.*, 2020, **56**, 12126-12129.
38 S. Nsanzamahoro, W. Cheng, F. P. Mutuyimana, L. Li, W. Wang, C. Ren, T. Yi, H. Chen and X. Chen, *Talanta*, 2020, **210**, 120636.
39 L. Zhao, H. Li, H. Liu, M. Liu, N. Huang, Z. He, Y. Li, Y. Chen and L. Ding, *Anal. Bioanal. Chem.*, 2019, **411**, 2373-2381.
40 C.-H. Zeng, X.-T. Meng, S.-S. Xu, L.-J. Han, S. Zhong and M.-Y. Jia, *Sens. Actuators B*, 2015, **221**, 127-135.
41 C. Zhao, X. Li, C. Cheng and Y. Yang, *Microchem. J.*, 2019, **147**, 183-190.
42 S. Liao, F. Zhu, X. Zhao, H. Yang and X. Chen, *Sens. Actuators B*, 2018, **260**, 156-164.
43 I. Alkian, H. Sutanto, B. Hadiyanto, A. Prasetio and B. Aprimanti Utami, *Cogent Eng.*, 2022, **9**, 2033467.

44 D. Bano, V. Kumar, S. Chandra, V. K. Singh, S. Mohan, D. K. Singh, M. Talat and S. H. Hasan, *Opt. Mater.*, 2019, **92**, 311-318.
45 X. Liu, S. Wei, Q. Diao, P. Ma, L. Xu, S. Xu, Y. Sun, D. Song and X. Wang, *Microchim. Acta*, 2017, **184**, 3825-3831.
46 L. Shi, D. Chang, G. Zhang, C. Zhang, Y. Zhang, C. Dong, L. Chu and S. Shuang, *RSC Adv*, 2019, **9**, 41361-41367.
47 L. Zhang, H. Wang, Q. Hu, X. Guo, L. Li, S. Shuang, X. Gong and C. Dong, *Microchim. Acta*, 2019, **186**, 1-13.
48 L. Sun, Y. Liu, Y. Wang, J. Xu, Z. Xiong, X. Zhao and Y. Xia, *Opt. Mater.*, 2021, **112**, 110787.
49 N. Wang, Z. X. Liu, R. S. Li, H. Z. Zhang, C. Z. Huang and J. Wang, *J Mater Chem B*, 2017, **5**, 6394-6399.
50 C.-L. Li, C.-C. Huang, A. P. Periasamy, P. Roy, W.-C. Wu, C.-L. Hsu and H.-T. Chang, *RSC Adv*, 2015, **5**, 2285-2291.
51 D. Kong, F. Yan, Z. Han, J. Xu, X. Guo and L. Chen, *RSC Adv*, 2016, **6**, 67481-67487.
52 M. Tian, Y. Liu, Y. Wang and Y. Zhang, *Anal. Methods*, 2019, **11**, 4077-4083.
53 G. Hu, L. Ge, Y. Li, M. Mukhtar, B. Shen, D. Yang and J. Li, *J. Colloid Interface Sci.*, 2020, **579**, 96-108.
54 Y.-L. Liu, L. Yang, L. Li, Y.-Q. Guo, X.-X. Pang, P. Li, F. Ye and Y. Fu, *Molecules*, 2019, **24**, 3093.
55 P. G. Mahajan, N. C. Dige, N. K. Desai, S. R. Patil, V. V. Kondalkar, S.-K. Hong and K. H. Lee, *Spectrochim Acta A Mol Biomol Spectrosc*, 2018, **198**, 136-144.
56 S.-F. Zhou, G.-M. Wu, T. Lin, C.-X. Zhang and Q.-L. Wang, *CrystEngComm*, 2020, **22**, 2013-2019.
57 X. Zhao, L. Wang, Q. Liu, M. Chen and X. Chen, *Microchem. J.*, 2021, **163**, 105888.
58 M. Tian, J. Zhang, Y. Liu, Y. Wang and Y. Zhang, *Spectrochim Acta A Mol Biomol Spectrosc*, 2021, **252**, 119541.
59 L. Wang, W. Li, L. Yin, Y. Liu, H. Guo, J. Lai, Y. Han, G. Li, M. Li and J. Zhang, *Sci. Adv.*, 2020, **6**, eabb6772.
60 L. Wang, M. Li, Y. Li, B. Wu, H. Chen, R. Wang, T. Xu, H. Guo, W. Li and J. Joyner, *Carbon*, 2021, **180**, 48-55.
61 Y. Zhang, R. Yuan, M. He, G. Hu, J. Jiang, T. Xu, L. Zhou, W. Chen, W. Xiang and X. Liang, *Nanoscale*, 2017, **9**, 17849-17858.
62 F. Yan, Z. Sun, H. Zhang, X. Sun, Y. Jiang and Z. Bai, *Microchim. Acta*, 2019, **186**, 1-37.
63 H. Guo, Z. Liu, X. Shen and L. Wang, *ACS Sustain. Chem. Eng.*, 2022, **10**, 8289-8296.
64 J. Liu, R. Li and B. Yang, *ACS Cent. Sci.*, 2020, **6**, 2179-2195.
65 J. C. Ahern, P. R. Ohodnicki Jr, J. P. Baltrus and J. L. Poole, "Luminescence based fiber optic probe for the detection of rare earth elements." U.S. Patent 11,170,986, November 9, 2021.
66 D. C. Harris, *Quantitative chemical analysis*, Macmillan, 2010.
67 M. P. Sk and A. Chattopadhyay, *RSC Adv*, 2014, **4**, 31994-31999.
68 N. D. Shooto, *Surf. Interfaces*, 2020, **20**, 100624.
69 A. Coutinho and M. Prieto, *J. Chem. Educ.*, 1993, **70**, 425.
70 M. Seferinoğlu, M. Paul, A. Sandström, A. Köker, S. Toprak and J. Paul, *Fuel*, 2003, **14**, 1721-1734.
71 S. E. Crawford, P. R. Ohodnicki and J. P. Baltrus, *J Mater Chem C*, 2020, **8**, 7975-8006.
72 S. Sinha, M. K. Mahata and K. Kumar, *New J. Chem.*, 2019, **43**, 5960-5971.
73 Y. Han, B. Tang, L. Wang, H. Bao, Y. Lu, C. Guan, L. Zhang, M. Le, Z. Liu and M. Wu, *ACS Nano*, 2020, **14**, 14761-14768.
74 F. Mocci, L. de Villiers Engelbrecht, C. Olla, A. Cappai, M. F. Casula, C. Melis, L. Stagi, A. Laaksonen and C. M. Carbonaro, *Chem. Rev.*, 2022, **122**, 13709–13799.
75 R. E. Ambrusi, J. Arroyave, M. E. Centurión, M. S. Di Nezio, M. F. Pistonesi, A. Juan and M. E. Pronsato, *Phys. E: Low-Dimens. Syst. Nanostructures*, 2019, **114**, 113640.
76 J. Yu, X. Yong, Z. Tang, B. Yang and S. Lu, *J. Phys. Chem. Lett.*, 2021, **12**, 7671-7687.
77 J. Ellis, S. Crawford and K.-J. Kim, *Mater. Adv.*, 2021, **2**, 6619-6196.
78 X.-L. Qu and B. Yan, *Inorg. Chem.*, 2018, **57**, 7815-7824.
79 W. Boonta, C. Talodthaisong, S. Sattayaporn, C. Chaicham, A. Chaicham, S. Sahasithiwat, L. Kangkaew and S. Kulchat, *Mater. Chem. Front.*, 2020, **4**, 507-516.
80 X. Xiao, L. Ren, S. Wang, Q. Zhang, Y. Zhang, R. Liu and W. Xu, *Fibers Polym.*, 2020, **21**, 2003-2009.
81 Y.-M. Zhu, C.-H. Zeng, T.-S. Chu, H.-M. Wang, Y.-Y. Yang, Y.-X. Tong, C.-Y. Su and W.-T. Wong, *J Mater Chem A*, 2013, **1**, 11312-11319.
82 Z. Wang, H. Liu, S. Wang, Z. Rao and Y. Yang, *Sens. Actuators B*, 2015, **220**, 779-787.
83 Q.-Q. Zhu, H. He, Y. Yan, J. Yuan, D.-Q. Lu, D.-Y. Zhang, F. Sun and G. Zhu, *Inorg. Chem.*, 2019, **58**, 7746-7753.
84 H. Wang, L. Yang, S. Chu, B. Liu, Q. Zhang, L. Zou, S. Yu and C. Jiang, *Anal. Chem.*, 2019, **91**, 9292-9299.

